European Cells and Materials Vol.47 2024 (pages 170–189) DOI: 10.22203/eCM.v047a12 ISSN 1473-2262

Original Article

A ROADMAP OF OSTEOGENIC DIFFERENTIATION IN HUMAN MESENCHYMAL STEM CELLS ASSESSED BY PROTEIN MULTIPLEX ANALYSIS

M. Eischen-Loges[1], Z. Tahmasebi Birgani[1], Y. Alaoui Selsouli[1], L. Eijssen[2], H. Rho[1], M. Sthijns[1,3], M. van Griensven[1], V. LaPointe[1,*,§] and P. Habibović[1,*,§]

[1]MERLN Institute for Technology-Inspired Regenerative Medicine, Maastricht University, 6200 MD, Maastricht, The Netherlands
[2]Department of Bioinformatics—BiGCaT, School of Nutrition and Translational Research in Metabolism (NUTRIM), Faculty of Health, Medicine and Life Sciences, Maastricht University, 6200 MD Maastricht, The Netherlands
[3]Food Innovation and Health, Department of Human Biology, Faculty of Health, Medicine and Life Sciences, School of Nutrition and Translational Research in Metabolism (NUTRIM), Maastricht University, 5928 SZ Venlo, The Netherlands

Abstract

Human mesenchymal stem cells (hMSCs) are widely used to model osteogenic differentiation *in vitro*, yet few studies compare the numerous available protocols. The poor translation between *in vitro* and *in vivo* results in bone regeneration highlights the need for improved methodologies to assess osteogenic phenotype. Omics technologies generate vast biological data but are complex for comparing several osteogenic differentiation strategies. Conversely, conventional methods like Alizarin red S stains or alkaline phosphatase assays do not provide enough data. Here, we propose a targeted protein multiplex assay to characterize and compare several models of osteogenic differentiation in hMSCs, containing markers for osteogenesis, angiogenesis, and inflammation—critical processes in bone regeneration. To induce osteogenic differentiation, hMSCs were stimulated with dexamethasone, with bone morphogenetic protein 2, supplemented with calcium or phosphate ions, or seeded on a calcium phosphate–based coating. Based on mineralization status determined by Alizarin red S stain, conditions were classified into non-mineralizing, late-mineralizing, and early-mineralizing groups. Protein patterns associated with these groups revealed distinct mechanisms of osteogenic differentiation for early- and late-mineralizing hMSCs. While non-mineralizing hMSCs did not undergo osteogenic differentiation, they exhibited increased angiogenic and inflammatory marker expression compared to the control. Late-mineralizing hMSCs had limited potential to produce angiogenesis-related factors, while early-mineralizing hMSCs showed an increased effect. Overall, we compared commonly used *in vitro* models of osteogenic differentiation in hMSCs to establish a comprehensive roadmap of osteogenic differentiation.

Keywords: Protein muliplex, human mesenchymal stem cells, osteogenic differentiation, calcium phosphate, mineralization.

***Address for correspondence**: Vanessa LaPointe, MERLN Institute for Technology-Inspired Regenerative Medicine, Maastricht University, 6200 MD, Maastricht, the Netherlands. Email: v.lapointe@maastrichtuniversity.nl; Pamela Habibović, MERLN Institute for Technology-Inspired Regenerative Medicine, Maastricht University, 6200 MD, Maastricht, the Netherlands. Email: p.habibovic@maastrichtuniversity.nl
[§]These authors contributed equally.

Introduction

Bone marrow–derived human mesenchymal stem cells (hMSCs) are multipotent progenitors, able to undergo differentiation towards the osteogenic, chondrogenic and adipogenic lineages (Bhat *et al.*, 2021; Xu *et al.*, 2017). They are of interest for tissue engineering and regenerative medicine, often in combination with a biomaterial, due to their role in regeneration and healing (Herberg *et al.*, 2021; Quade *et al.*, 2020; Sha *et al.*, 2019). For example, hMSCs have been shown to secrete biologically active factors with immunoregulatory, tissue-supportive, and instructive functions *in vitro* (Kehl *et al.*, 2019; Quade *et al.*, 2020; Shin *et al.*, 2021), and have successfully generated bone tissue, promoted host vascularization, and provided an immunomodulatory effect upon transplantation in several *in vivo* models (Clark *et al.*, 2020; Quade *et al.*, 2020; Taylor *et al.*, 2019). Despite these successes, the clinical application of hMSCs, for example in bone regeneration, remains limited. A reason for this is the difficulty to translate findings from *in vitro* work to *in vivo*, suggesting the need to

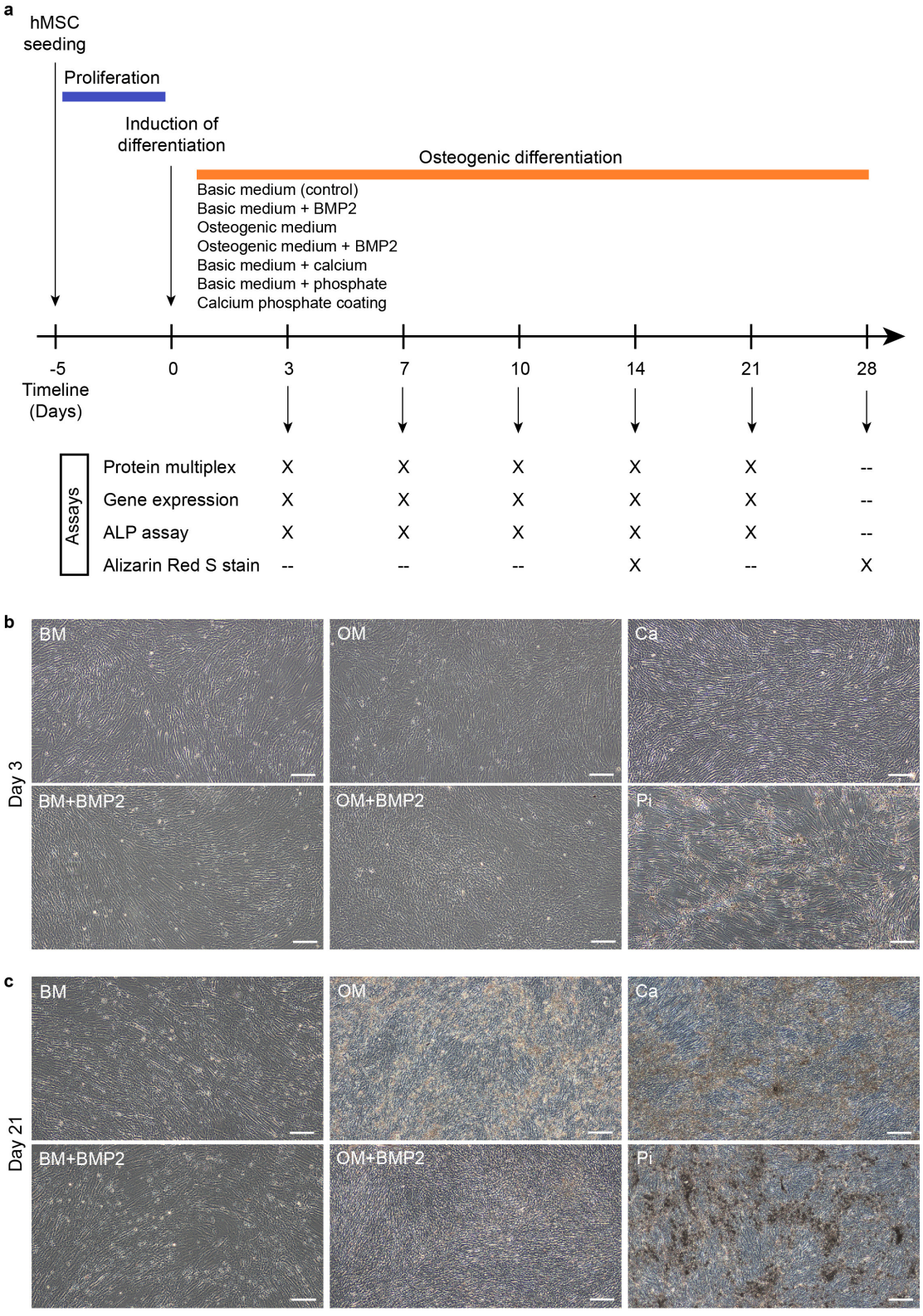

Fig. 1. Schematic overview of experimental set-up and cell morphology. (**a**) Different strategies were used to induce osteogenic differentiation in human mesenchymal stem cells (hMSCs) over 28 days. After mineralization assessment by Alizarin red S staining at days 14 and 28, the strategies were classified according to their resulting mineralization status into inducers of non-, late- and early-mineralization, and protein patterns from the multiplex assay were correlated to the mineralization status. Assays that were executed on a specific time point are marked by X. (**b**) Cell morphology and mineral deposition at day 3. Initial mineral deposits were observed in hMSCs in phosphate ions (Pi) at day 3. (**c**) Mineral deposits at day 21 were observed in hMSCs cultured in OM, OM+BMP-2, calcium (Ca), and Pi at day 21. Scale bar: 100 µm.

reconsider how differentiation of hMSCs is investigated *in vitro* (Hulsart-Billström *et al*., 2016). In particular, hMSC differentiation into the osteogenic lineage is important for bone regeneration and its application to heal critical-sized bone defects, which are currently treated by bone grafting, a common surgical procedure that is performed over 2.2 million times per year worldwide (Calori *et al.*, 2011).

A lot of effort has been put into finding a method to stably and reproducibly differentiate hMSCs, resulting in several *in vitro* strategies to direct their osteogenic differentiation. While three-dimensional (3D) models have demonstrated the ability to more accurately mimic the physiological environment of bone, overcoming the limitations associated with two-dimensional (2D) models such as forced polarity and reduced cell-cell contacts, the use of 2D models in the field remains high (Braccini *et al.*, 2005). This study will focus on commonly used 2D models within the field. Common medium components include dexamethasone to enhance alkaline phosphatase (ALP) expression, β-glycerophosphate to serve as a phosphate source for mineralization, and ascorbic acid as a co-factor for collagen synthesis (Sordi *et al.*, 2021). Dexamethasone is typically supplemented throughout the culture at a concentration range that varies (e.g., from 10 nM to 1 µM) in different studies. Growth factors such as bone morphogenetic protein-2 (BMP2), bone morphogenetic protein-7 (BMP7), bone morphogenetic protein-9 (BMP-9) or transforming growth factor beta-1 (TGF-beta-1) are also used to upregulate pathways related to osteogenesis (Han *et al.*, 2020; Xu *et al.*, 2020; Yang *et al.*, 2018). Osteogenic differentiation can also be achieved through the enrichment of medium with calcium (Ca) or phosphate ions (Pi), or by culturing cells on calcium phosphate (CaP) scaffolds (Danoux *et al.*, 2015; Lei *et al.*, 2015).To date, there are few experimental studies comparing the considerable number of differentiation protocols available, and there is a lack of standardization in the methodologies used to assess the osteogenic phenotype.

When choosing the methodology to assess a phenotype, there are several important considerations. Conventional assays such as Alizarin red S (ARS) staining, quantitative RT-PCR and ALP assays are affordable and easy to perform, but provide limited biological information, which may contribute to the poor (pre-) clinical translation of *in vitro* findings (Hulsart-Billström *et al.*, 2016). Alternatively, numerous studies have investigated the protein profiles of hMSCs using omics technologies (Kehl *et al.*, 2019; Lei *et al.*, 2015; Shin *et al.*, 2021), which generate a large amount of biological data that can provide important insights. However, these methods are complex, expensive and require specialized infrastructure. A protein multiplex analysis could be considered a promising intermediate tool to characterize hMSCs *in vitro* as it is a simple assay that can simultaneously quantify a panel of selected proteins, making it a more targeted and cost-effective approach. The use of multiplex protein assays remains limited in tissue engineering, though a study by Fischer *et al.* (2022) evaluated the effect of cold physical plasma on osteogenic differentiation of hMSCs and used a 12-plex assay comprising cytokines, chemokines and growth factors at early time points (Fischer *et al.*, 2022).

Here, we used a targeted proteomic approach with an 18-plex panel of markers for osteogenesis, angiogenesis, and inflammation in hMSCs. Osteogenic differentiation was induced using different strategies, which were then classified as non-, early- and late-mineralizing groups according to the resultant mineralization status (Fig. 1). Protein expression patterns were then associated with the different classifications. We identified osteogenic markers, such as matrix metalloproteinase-13 (MMP-13) and growth arrest-specific 6 (GAS-6), that could be correlated to the mineralization status, while others such as TGF-beta-1 were inversely correlated. We also showed higher angiogenic potential and increased inflammatory markers in hMSCs that did not mineralize. Based on our results, we consider a targeted protein multiplex assay as a practical tool to characterize differentiating hMSCs and to provide a better understanding of osteogenic differentiation *in vitro*, both informing the more effective use of hMSCs in regenerative medicine.

Materials and Methods

Calcium Phosphate Coating Preparation

For the first coating step, a five-times concentrated simulated body fluid solution was prepared by dissolving carbon dioxide (CO_2) gas into a solution comprising 733.5 mM Na^{2+}, 7.5 mM Mg^{2+}, 12.5 mM Ca^{2+}, 720 mM Cl^{-}, 5 mM $HPO_4{}^{2-}$, and 21 mM $HCO_3{}^{-}$ in demineralized water at 37 °C, made from reagent grade NaCl, $CaCl_2{\cdot}2H_2O$, $MgCl_2{\cdot}6H_2O$, $Na_2HPO_4{\cdot}2H_2O$ and $NaHCO_3$ salts, added one after the other, as previously described (Yang *et al.*, 2010). The solution was sterile-filtered and 6-well tissue culture plates (Corning, Amsterdam, The Netherlands) were filled with 2 mL of the solution and incubated at 37 °C in 5 % CO_2 for 24 h, resulting in the formation of an amorphous CaP layer. The plates were washed twice with cell culture grade water.

In the second coating step, CO_2 was dissolved into a solution comprising 733.5 mM Na^{2+}, 1.5 mM Mg^{2+}, 12.5 mM Ca^{2+}, 720 mM Cl^{-}, 5 mM $HPO_4{}^{2-}$, and 10 mM $HCO_3{}^{-}$, made from reagent grade NaCl, $CaCl_2{\cdot}2H_2O$, MgCl2·6H_2O, $NaHCO_3$ and $Na_2HPO_4{\cdot}2H_2O$ salts, added one after the other, in demineralized water at 50°C to prepare a second five-times concentrated simulated body fluid solution with a decreased concentration of Mg^{2+} and $HCO_3{}^{-}$ (Yang *et al.*, 2010). The solution was sterile-filtered and the 6-well tissue culture plates (Corning) were filled with 2 mL of the solution and incubated at 37 °C in 5 % CO_2 for 3 days with daily refreshments, resulting in the formation of a crystalline CaP layer. Following the coating process, the plates were washed twice with cell culture

Table 1. Primer sequences.

Target gene	Accession nr.	Primer sequence (5′–3′)	RT-PCR product size (bp)
RPL13A	NM_001270491.2	F: GCCCTACGACAAGAAAAAGCG R: TACTTCCAGCCAACCTCGTGA	117
YWHAZ	NM_001135699.2	F: CCTGCATGAAGTCTGTAACTGAG R: GACCTACGGGCTCCTACAACA	100
RUNX2	NM_001015051.4	F: TCAACGATCTGAGATTTGTGGG R: GGGGAGGATTTGTGAAGACGG	81
OSX	NM_001173467.3	F: CCTCTGCGGGACTCAACAAC R: AGCCCATTAGTGCTTGTAAAGG	128
BMP2	NM_001200.4	F: ACTACCAGAAACGAGTGGGAA R: GCATCTGTTCTCGGAAAACCT	113
ALP	NM_000478.6	F: ACAAGCACTCCCACTTCATC R: TTCAGCTCGTACTGCATGTC	112
SPP1	NM_000582.3	F: GAAGTTTCGCAGACCTGACAT R: GTATGCACCATTCAACTCCTCG	91
COL1A1	NM_000088.4	F: GTGCGATGACGTGATCTGTGA R: CGGTGGTTTCTTGGTCGGT	119
OCN	NM_199173.6	F: TGAGAGCCCTCACACTCCTC R: CGCCTGGGTCTCTTCACTAC	151

grade water. Before cell seeding, the CaP coatings were sterilized in 100 % isopropanol for 2 min and 70 % isopropanol for 2 min, washed twice in cell culture grade water, and soaked in basic medium (BM) for 30 min.

Fourier-Transform Infrared Spectroscopy

CaP-coated well plates were washed twice with cell culture grade water and dried. Attenuated total reflectance Fourier-transform infrared spectroscopy (ATR-FTIR) (Nicolet is50, Thermo Fisher Scientific, Landsmeer, The Netherlands) was performed in the range of 500–4500 cm^{-1} in the transmission mode in order to identify structural groups.

X-Ray Diffraction (XRD) Analysis

Phase analysis and the degree of crystallinity of the CaP coatings were determined on an X-ray diffractometer (D2; Bruker) at room temperature in the range of $6 \leq 2\theta \leq 60$ with a scan rate of 1°/min and a step size of 0.03°. Pattern analysis was performed using Profex 4.2. (Solothurn, Switzerland) (Doebelin and Kleeberg, 2015).

Scanning Electron Microscopy (SEM) and Energy-Dispersive X-Ray Spectroscopy (EDS) Analyses

The coated wells were washed, cut, and glued onto aluminum stubs using carbon tape, after which they were gold sputter coated (SC7620, Quorum Technologies, Laughton, England). To visualize the CaP crystal morphology and their distribution on the surface of the coating, scanning electron microscopy (JSM-IT200, JEOL, Zaventem, Belgium) was performed at an acceleration voltage of 20 kV and magnifications of up to 10,000×. To determine the elemental composition of the coating and its homogeneity, energy-dispersive X-ray spectroscopy analysis (JSM-IT200, JEOL) was performed.

hMSC Culture

HMSCs originating from bone marrow were obtained from PromoCell on 27-11-2019 (Lot: 451Z021.2) (PromoCell, Huissen, The Netherlands, 65-year-old donor), with confirmed marker expression of CD73, CD90, and CD105 and absence of CD14, CD19, CD34, CD45, and HLA-DR markers, as recommended by the International Society for Cellular Therapy and free from any contaminants such as bacteria, fungi and mycoplasma. Cells at passage 2 were seeded at 2000 cells/cm^2 in BM composed of minimal essential medium (α-MEM GlutaMAX no nucleosides; Gibco, Landsmeer, The Netherlands) supplemented with 10 % fetal bovine serum, and were maintained in a humidified environment at 37 °C in 5 % CO_2. Medium was changed every two days. Upon reaching 80 % confluence, cells were detached using 0.05 % trypsin-EDTA and reseeded at a density of 1000 cells/cm^2 for further expansion. Cells were used for experiments after passage 4, when they were seeded into 6-well plates (Corning) with or without CaP coatings at a density of 10,000 cells/cm^2 in 2 mL of BM. Prior to inducing osteogenic differentiation, cells were expanded to confluence.

Trilineage Differentiation Potential of hMSCs

Adipogenic differentiation was induced in hMSCs which were seeded at a density of 10,000 cells/cm^2. After a 2-day expansion, adipogenic medium consisting of Dulbecco's modified Eagle medium (high glucose, no sodium pyruvate; Gibco, Landsmeer, The Netherlands) supplemented with 10 % FBS, 40 mM indomethacin, 83 mM 3-

isobutyl-1-methylxanthine, 10 mg/mL insulin and 0.1 mM dexamethasone was added. Medium was changed every 2–3 days. After 21 days, cells were fixed in 4 % wt/vol paraformaldehyde for 15 min at room temperature. Cells were stained with a 0.2 % (wt/vol) Oil Red O solution in 60 % isopropanol for 15 min to detect lipid droplets. Chondrogenic differentiation was induced in hMSCs which were seeded at a density of 200,000 cells per well in a 96-well, U-bottom suspension culture plate. Aggregates formed within 24 h. Chondrogenic differentiation medium consisting of Dulbecco's modified Eagle medium (high glucose, no sodium pyruvate; Gibco) supplemented with 10 % FBS, 50 mg/mL ITS premix (Thermo Fisher Scientific, Landsmeer, The Netherlands), 40 µg/mL proline, 0.2 mM ascorbic acid phosphate, 100 µg/mL sodium pyruvate, 0.1 µM dexamethasone and 10 ng/mL TGF-b3 (PeproTech, Hamburg, Germany) was added. Medium was changed every two days. After 21 days in culture, aggregates were fixed in 4 % wt/vol paraformaldehyde for 25 min at room temperature. Aggregates were embedded in paraffin, sectioned, rehydrated and stained with 1 % Alcian blue solution in acetic acid for 30 min in order to detect proteoglycans. Osteogenic differentiation was induced in hMSCs in osteogenic medium (OM), with the formulation described in the next section. The capacity of hMSCs to mineralize, as an indicator for osteogenic differentiation, was assessed via ARS staining at day 28 of culture.

Osteogenic Differentiation

HMSCs were exposed to seven different conditions: (1) BM as a reference condition, (2) BM supplemented with 50 ng/mL BMP2 (PeproTech) (BM+BMP2), (3) OM consisting of BM supplemented with 0.01 M β-glycerophosphate, 0.2 mM ascorbic acid, and 0.1 µM dexamethasone, (4) OM supplemented with 50 ng/mL BMP2 (OM+BMP2), (5) BM supplemented with a final concentration of 8 mM calcium (Ca) from a 100× stock solution consisting of demineralized water, 25 mM HEPES, 140 mM NaCl, and 620 mM $CaCl_2$, (6) BM supplemented with a final concentration of 8 mM phosphate (Pi) from a 100× stock solution consisting of demineralized water, 25 mM HEPES, 140 mM NaCl, and 680 mM of phosphate (pH neutral mixture of NaH_2PO_4 and Na_2HPO_4), and (7) hMSCs seeded directly on sterile CaP coatings at 10,000 cells/cm^2 in BM. They were analyzed at five time points (days 3, 7, 10, 14 and 21). Ca and Pi concentrations surpassed physiological levels, however, previous studies have their capacity to induce robust osteogenic responses (Aquino-Martínez *et al.*, 2017; Lee *et al.*, 2018; McCullen *et al.*, 2010).

Multiplex Analysis

An 18-plex bead-based immunoassay panel (ProcartaPlex custom panel, Invitrogen, Waltham, MA USA) was performed to quantify protein concentrations. The panel was composed of osteogenic markers: BMP-2, BMP-9, fibroblast growth factor-23 (FGF-23), osteopontin (SPP-1), osteoprotegerin (OPG), receptor activator of NF-κB ligand (RANKL), growth arrest-specific protein 6 (GAS-6), MMP-13, TGF-beta-1 and tenascin-C (TN-C); angiogenic markers: angiopoietin-1 (ANG-1), vascular endothelial growth factor A (VEGF-A); inflammation markers: interleukin-6 (IL-6), Tumor necrosis factor ligand superfamily member 2 (TNF-A), granulocyte-macrophage colony-stimulating factor (GM-CSF); and some other markers: 5′-nucleotidase (CD73), calcitonin (CALCA) and L-lactate dehydrogenase B (LDH-B) which are related to stemness, calcium metabolism, and cell viability, respectively. A separate single-plex assay for TGF-beta-1 was done as this microbead population could not be combined with others. Protein concentration was measured in the cell culture supernatant at time points 0, 3, 7, 10, 14 and 21 days, as well as in the lysate of the same samples.

For lysis, the cells were washed twice with phosphate buffered saline (PBS) and frozen at – 80 °C. After three freeze–thaw cycles at – 80 °C, 500 µL of lysis buffer (ProcartaPlex, Invitrogen, Waltham, MA USA) supplemented with 1 mM phenylmethylsulfonyl fluoride was added to each well and incubated for 15 min on ice before collection. Samples were sonicated three times for 10 s. The immunoassay panel was performed according to the manufacturer's instructions. In brief, samples were diluted 2× in the universal assay buffer provided in the kit, and 50 µL of medium supernatant or cell lysate from each sample, along with standards and quality controls, were added to wells containing the antibody-coupled beads, shaken for 30 min at room temperature, incubated overnight at 4 °C, and shaken again for 30 min. After two washing steps, detection antibody–biotin reporters were added to each well and incubated for 30 min at room temperature with shaking, followed by incubation with the fluorescent conjugate streptavidin–phycoerythrin for 30 min while shaking. Protein concentrations were measured using a Luminex100 (Bio-Rad, Veenendaal, The Netherlands) with data acquisition in Bio-Plex Manager 6.0 software (Bio-Rad, Veenendaal, The Netherlands). Calibration and verification were performed before analysis. Standard curves were established for each analyte with known concentrations of proteins, and the concentrations of analyzed markers were expressed as picograms per milliliter (pg/mL). Blanks containing cell culture medium or lysis buffer and a known sample as quality control were analyzed in each assay in duplicate. For normalization of protein concentration, a single-plex assay for HSP60, a housekeeping protein, was done following the same steps. Each protein concentration normalized to HSP60 is represented as a ratio relative to expression at day 0.

Alizarin Red S Staining and Quantification

Alizarin red analysis was performed at days 14 and 21, for which hMSCs were washed twice with PBS and fixed

in 4 % (wt/vol) paraformaldehyde for 15 min at room temperature. After three washes in distilled water, cells were stained with 2 % (wt/vol) Alizarin red S solution in distilled water (pH 4.2) for 15 min with gentle shaking. Calcium deposits, stained in red, were imaged by phase contrast microscopy. For colorimetric quantification, Alizarin red S staining was removed by incubation in 10 % hexadecylpyridinium chloride in 10 mM sodium phosphate buffer (pH 7.0) overnight at room temperature. The dissolved solution was transferred to a 96-well plate, diluted if necessary, and the absorbance was measured at 562 nm on a plate reader (CLARIOstar, BMG Labtech, Ortenberg, Germany). A standard curve with known amounts of Alizarin red S was used to estimate sample concentrations. Control wells without cells that had received the same treatments, and a CaP coating without cells, were used as a blank measurement for the different conditions and subtracted from experimental measurements.

Alkaline Phosphatase Activity Assay

ALP levels were measured to indicate osteoblast phenotype at days 3, 7, 10, 14 and 21 of culture. Cell lysis was done as previously described, and ALP activity was quantified using the CDP-Star solution (Sigma-Aldrich, Amsterdam, The Netherlands) (Alves *et al.*, 2011; Zhang *et al.*, 2014). The cell lysate was incubated 1:5 with the reagent for 20 min in the dark at room temperature in a white-bottom 96-well plate. Luminescence was read on a spectrophotometer (CLARIOstar, BMG Labtech, Ortenberg, Germany) with a 3600 gain and a measurement interval of 1 s. ALP values were normalized to the housekeeping protein HSP60 expression.

RT-qPCR

Samples were lysed in TRIzol at days 3, 7, 10, 14 and 21. RNA was extracted using the phenol chloroform method and purified using a Bioline kit. RNA purity and quantity were determined on a BioDrop. For each sample, 500 ng of RNA were reverse transcribed into cDNA using the iScript cDNA synthesis kit (Bio-Rad, Veenendaal, The Netherlands). The amplification of 20 ng of cDNA by qRT-PCR was performed on a CFX96 Real-Time PCR Detection System using the iQ SYBR Green Supermix (Bio-Rad, Veenendaal, The Netherlands). Transcript levels of osteogenic biomarkers including runt-related transcription factor 2 (*RUNX2*), osterix (*OSX*), *BMP2*, *ALP*, *SPP1*, collagen type I alpha 1 chain (*COL1A1*), and osteocalcin (*OCN*), were determined. Fold expression values were determined using the ΔΔCt method after normalizing each target gene with respect to the geometric mean of the expression of two stably-expressed housekeeping genes (*RPL13A* and *YWHAZ*) and to the expression of the target gene in hMSCs at day 0 on culture plates in BM. Primer sequences can be found in Table 1.

Statistical Analysis

Two-way analysis of variance (ANOVA) was done on all data sets, except the protein data. Data are represented as mean ± standard deviation. Post-hoc analysis was performed using Dunnett's test. p-values < 0.05 were considered statistically significant.

Concerning the statistical analysis of the protein data, missing data points below the detection limit of the Luminex instrument were imputed using the lowest concentration of the standard curve of the corresponding protein or the lowest value in the data set if the latter was below the standard curve value. Missing data points above the detection limit were imputed using the highest value of the standard curve of the corresponding protein or the highest value in the data set if the latter was above the standard curve value. The proteins SPP-1 in the lysate and CALCA in the lysate had too many missing values, and were therefore removed before analysis. After data preprocessing, differential expression analysis on protein data was done using linear regression modelling on a log scale (DEP package 1.21.0 in R 4.2.0). p-values were computed using the Benjamini-Hochberg false discovery rate correction for multiple tests (p.adjust function in R). Principal component analysis (PCA) was performed per time point and per group of proteins (osteogenesis-, angiogenesis- or inflammation-related) in order to determine sample clustering and whether different experimental groups showed a different osteogenic, angiogenic or inflammatory marker expression.

Results

A Carbonated Apatite Coating was Deposited on Well Plates

SEM analysis of the CaP-coated tissue culture plates showed that a homogenous mineral layer was deposited (Fig. 2**a**). ATR-FTIR spectroscopy showed the presence of phosphate and carbonate bands (Fig. 2**b**). The XRD pattern was typical of a crystalline carbonated apatite (Fig. 2**c**).

hMSCs were able to Undergo Trilineage Differentiation

The trilineage differentiation potential of the hMSCs was evaluated. Positive staining for Oil red O, Alizarin red S, and Alcian blue confirmed their capacity to differentiate into adipocytes, osteoblasts, and chondrocytes, respectively (Fig. 2**d**).

Increased Mineral Deposition was Detected in hMSCs in OM, OM+BMP-2, Ca, Pi and on CaP

HMSCs were subjected to seven different conditions: BM, which served as a non-differentiating control, BM+BMP2, OM, OM+BMP2, Ca, Pi and on CaP. Morphological changes and mineral deposition patterns in hMSCs were examined over the course of culture time. Initially, mineral deposits were observed in hMSCs in Pi early as day 3 (Fig. 1**b**). At day 21, mineral deposits were ob-

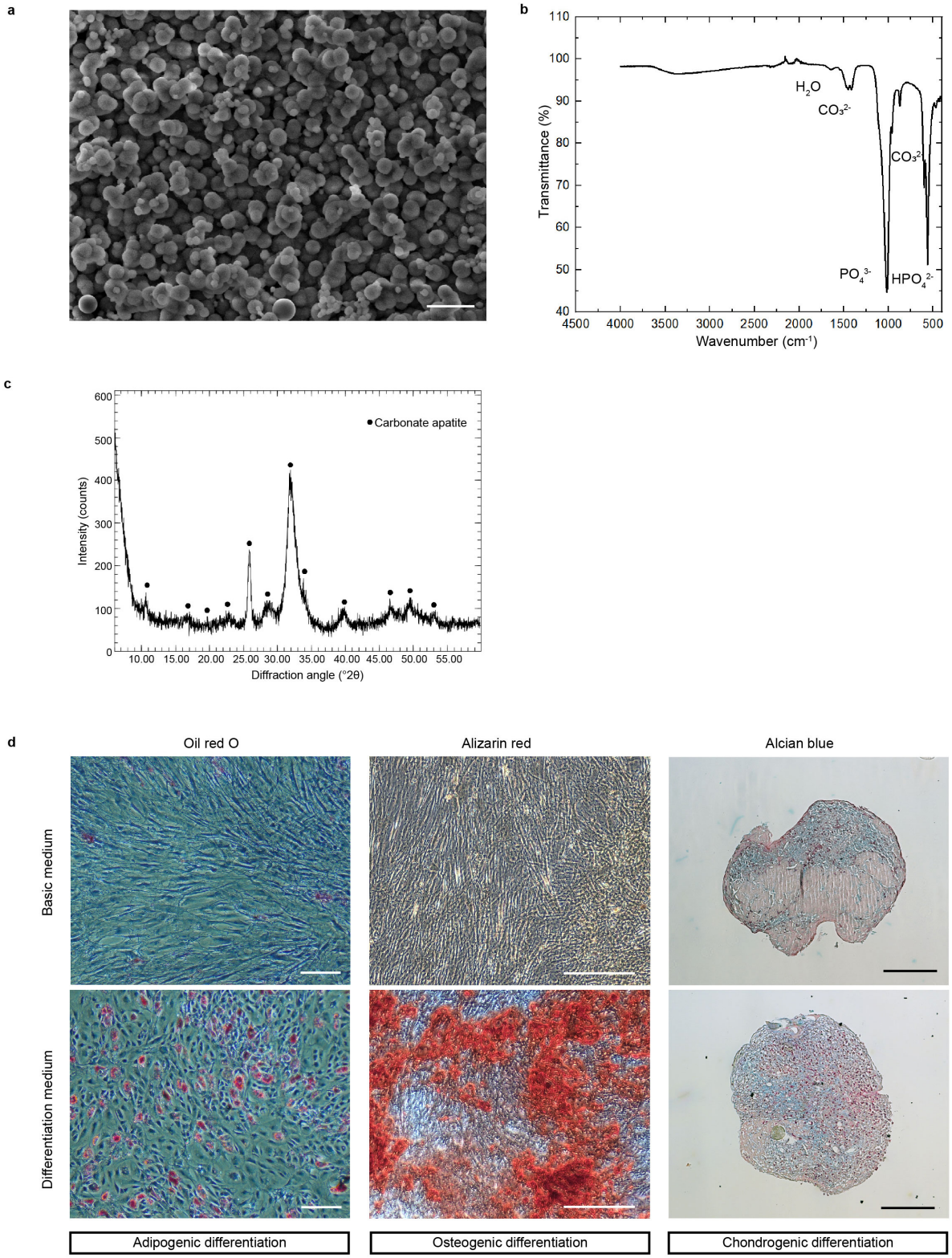

Fig. 2. Characterization of calcium phosphate (CaP) coating and of hMSCs. (**a**) A homogenous CaP coating was deposited as observed by scanning electron microscope. Scale bar: 10 µm. (**b**,**c**) Attenuated total reflectance Fourier-transform infrared spectroscopy (ATR-FTIR) spectrum and X-Ray Diffraction (XRD) pattern show a carbonated apatite. (**d**) hMSCs are able to undergo trilineage differentiation as show by Oil red O stain at day 21 of culture, Alizarin red S stain at day 28 of culture and Alcian blue stain at day 21 of culture. Scale bars: 100 µm, 100 µm and 200 µm, respectively.

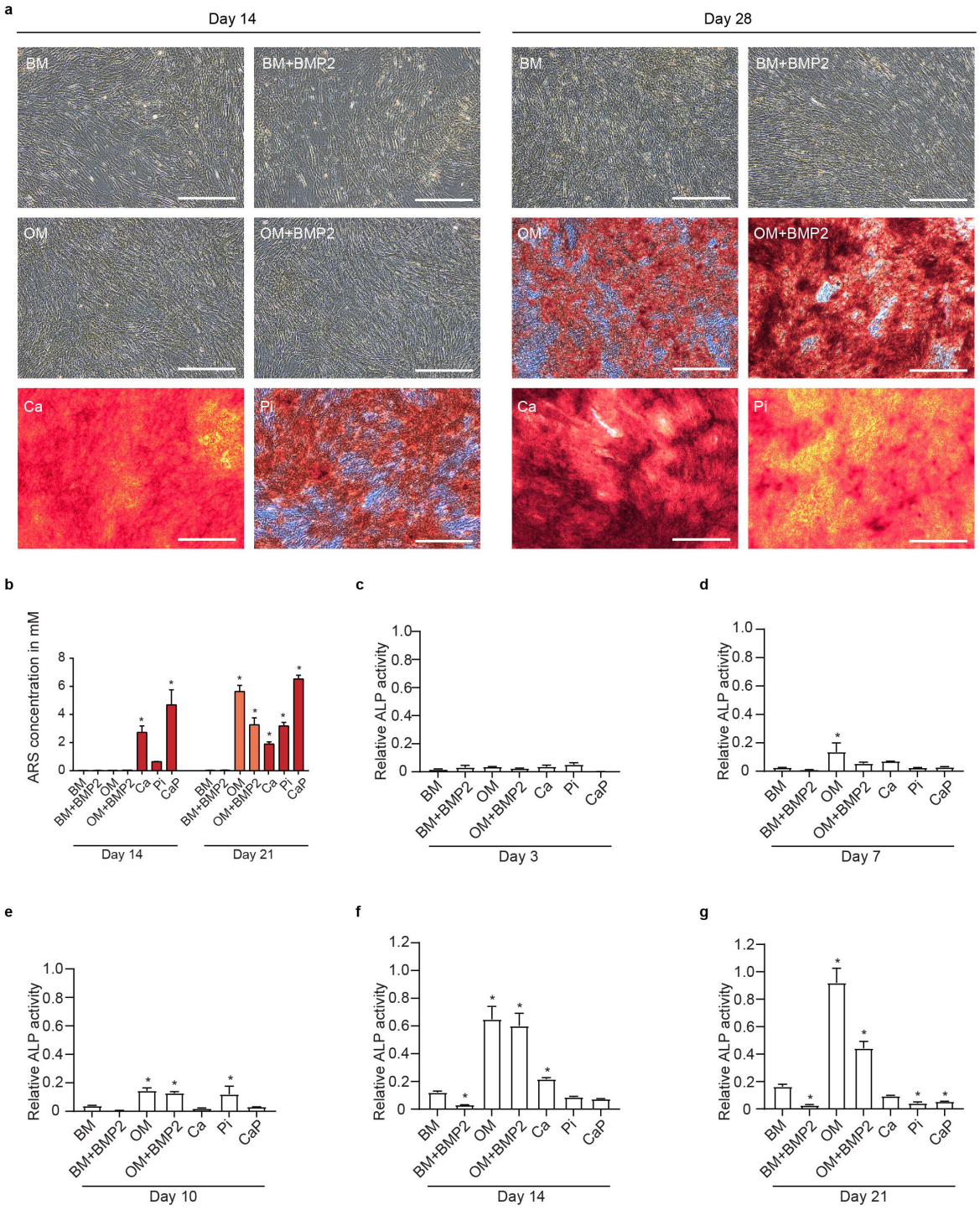

Fig. 3. Increased mineralized matrix was formed in hMSCs in OM, OM+BMP2, Ca, Pi and on CaP, while ALP activity was increased only in hMSCs in OM and OM+BMP2. Phase contrast images of hMSCs stained with Alizarin red S after 14 and 28 days in culture to visualize mineral deposits (**a**). Data are representative of at least three independent experiments (N = 3) with similar results. Scale bars represent 100 µm. The stain was quantified (**b**) to classify the conditions as non-mineralizing (basic medium (BM) and BM+BMP2), early-mineralizing (Ca, Pi and CaP) or late-mineralizing (OM and OM+BMP2). ALP activity was quantified after 3, 7, 10, 14 and 21 days in culture (**c-g**) relative to a housekeeping protein (HSP60) set to 1.0. ALP activity relative to the BM control was decreased in hMSCs in BM+BMP2 after 14 and 21 days. It was increased in hMSCs in OM beginning on day 7, in OM+BMP2 beginning on day 10, in Ca beginning on day 14, and in Pi at day 10. At day 21, ALP activity in hMSCs in Pi and on CaP was decreased relative to the control. Bars represent the mean of three independent experiments (N = 3), error bars represent standard deviation and * indicates $p < 0.05$ relative to BM.

served in hMSCs cultured in OM, OM+BMP2, as well as in Ca and Pi (Fig. 1**c**). Taking phase contrast images of hMSCs through the thick CaP coating was not feasible due to technical limitations. Increased osteogenic differentiation, as defined by mineral deposition, was confirmed by a positive Alizarin red S stain in hMSCs in Ca and Pi and on CaP after 14 days in culture and in OM and OM+BMP2 after 28 days in culture (Fig. 3**a**). The Alizarin red S stain was then dissolved and quantified (Fig. 3**b**). After 14 days in culture, the amount of Alizarin red S in hMSCs in Ca (2.7 mM ARS) and on CaP (4.7 mM ARS) was higher (all $p < 0.001$) than that in the BM control (0.026 mM ARS), while the amount in BM+BMP2, OM, OM+BMP2 and Pi was not significantly different from the control. After 28 days in culture, the amount from hMSCs in OM (5.6 mM ARS), OM+BMP2 (3.3 mM ARS), Ca (1.9 mM ARS), and Pi (3.2 mM ARS) and on CaP (6.5 mM ARS) was higher (all $p < 0.001$) relative to hMSCs in BM (0.035 mM ARS) (Fig. 3**b**). These findings led us to classify the osteogenic differentiation conditions into three groups, namely "non-mineralization" (in BM+BMP2), "late-mineralization" (in OM and OM+BMP2) and "early-mineralization" (in Ca and Pi, and on CaP).

Increased Alkaline Phosphatase Activity was Detected in HMSCs in OM, OM+BMP2, Ca and Pi

ALP activity, an enzyme known to promote mineralization that is upregulated in the early stages of osteoblast commitment, was measured at days 3, 7, 10, 14 and 21 (Fig. 3**c-g**). As expected, increased ALP activity was detected to be above the level of the BM control in both the early- and late-mineralization groups, albeit at time points that did not necessarily correspond to their mineralization. After 3 days in culture, there were no significant changes (Fig. 3**c**) compared to hMSCs in BM, but ALP activity was increased after 7 days in OM (Fig. 3**d**), and after 10 days in OM, OM+BMP2 and Pi (Fig. 3**e**). After 14 days, ALP activity was increased in OM, OM+BMP2, and Ca, and decreased in hMSCs in BM+BMP2 compared to the BM control (Fig. 3**f**). After 21 days, ALP activity was increased in hMSCs in OM and OM+BMP2, and decreased in BM+BMP2 and Pi, and on CaP (Fig. 3**g**).

A Multiplex Assay to Determine hMSC Phenotype when Differentiating towards the Osteogenic Lineage

An 18-plex protein multiplex assay was performed at days 3, 7, 10, 14 and 21 on the cell lysates (LY) and/or the medium supernatants (SN), depending on the protein, in order to establish protein profiles for the different conditions (Fig. 4**a**). At each time point, differential expression analysis determined significant changes relative to control hMSCs in BM. To identify potential protein expression patterns between groups, PCA analysis was performed using the abundances of the proteins, grouped as osteogenic, angiogenic and inflammatory markers, for each time point. The PCA was plotted based on the first and second principal. The contribution of proteins to principal components can be found in Fig. 5**a-c**. An overview of the significant markers can be found in Fig. 6**d**.

MMP-13 and GAS-6 in Cell Lysates Correlated with Mineralization Status while MMP-13, GAS-6 and TGF-beta-1 in Cell Supernatant Inversely Correlated with Mineral Deposition

Twelve markers were analyzed in order to characterize osteogenic differentiation in hMSCs: CD73, TN-C, MMP-13, SPP-1, GAS-6, BMP-9, FGF-23, RANKL, OPG, BMP-2, TGF-beta-1 and CALCA (Fig. 4**a**,**b**, Fig. 6**a**).

As expected, hMSCs that had been classified as non-mineralizing (BM+BMP2) formed a well-defined cluster at most time points. Compared to hMSCs in BM, this cluster at day 3 was defined by an increase in SPP-1, BMP-9, FGF-23, RANKL and OPG, all in the supernatant. And at day 7, this cluster expressed an increase of TGF-beta-1, GAS-6, MMP-13, RANKL, SPP-1 and BMP-9, all in the supernatant. By day 10, the non-mineralization group was showing more similarities to hMSCs in OM+BMP2. This correlation was determined by an increase of BMP-9, SPP-1 and FGF-23, and a decrease in BMP-2, all in the supernatant. As time continued to days 14 and 21, the non-mineralization group was the least correlated to the other conditions. This was determined by an increase in TGF-beta-1, FGF-23, BMP-9, and OPG at day 14, all in the supernatant and a decrease of TN-C in the lysate, and by an increase of OPG and TGF-beta-1 in the supernatant, and a decrease of TN-C, MMP-13 and OPG in the lysate at day 21.

The group of late-mineralizing hMSCs clustered together with the control in BM at day 3. However, both conditions belonging to the late-mineralizing condition did not cluster closely together until day 14 and we noted significant differences between hMSCs in OM compared to OM+BMP2, despite their similar timelines of mineralization and ALP activity. For example, at day 7, hMSCs in OM+BMP2 were defined by the increase of MMP-13 in the lysate, and FGF-23 and BMP-9 in the supernatant, while OPG in the lysate decreased. The two conditions diverged further at day 10, where FGF-23 and BMP-9 in the supernatant were decreased in OM and increased in OM+BMP2. The OM+BMP2 condition was further defined by the increase in MMP-13 in the lysate, which was not seen in hMSCs in OM. By day 14, the two conditions in the late-mineralization group converged. HMSCs in OM expressed diminished osteogenic markers, namely TGF-beta-1, FGF-23 and BMP-9, all in the supernatant, and TN-C in lysate. Conversely, hMSCs in OM+BMP2 were defined by an increase of MMP-13 (in both the supernatant and lysate), and a decrease in BMP-2 in the supernatant and OPG in the lysate. TN-C in lysate was also decreased. Despite these differences, the overall profile of the two conditions was similar, and this trend continued until day 21, at which point

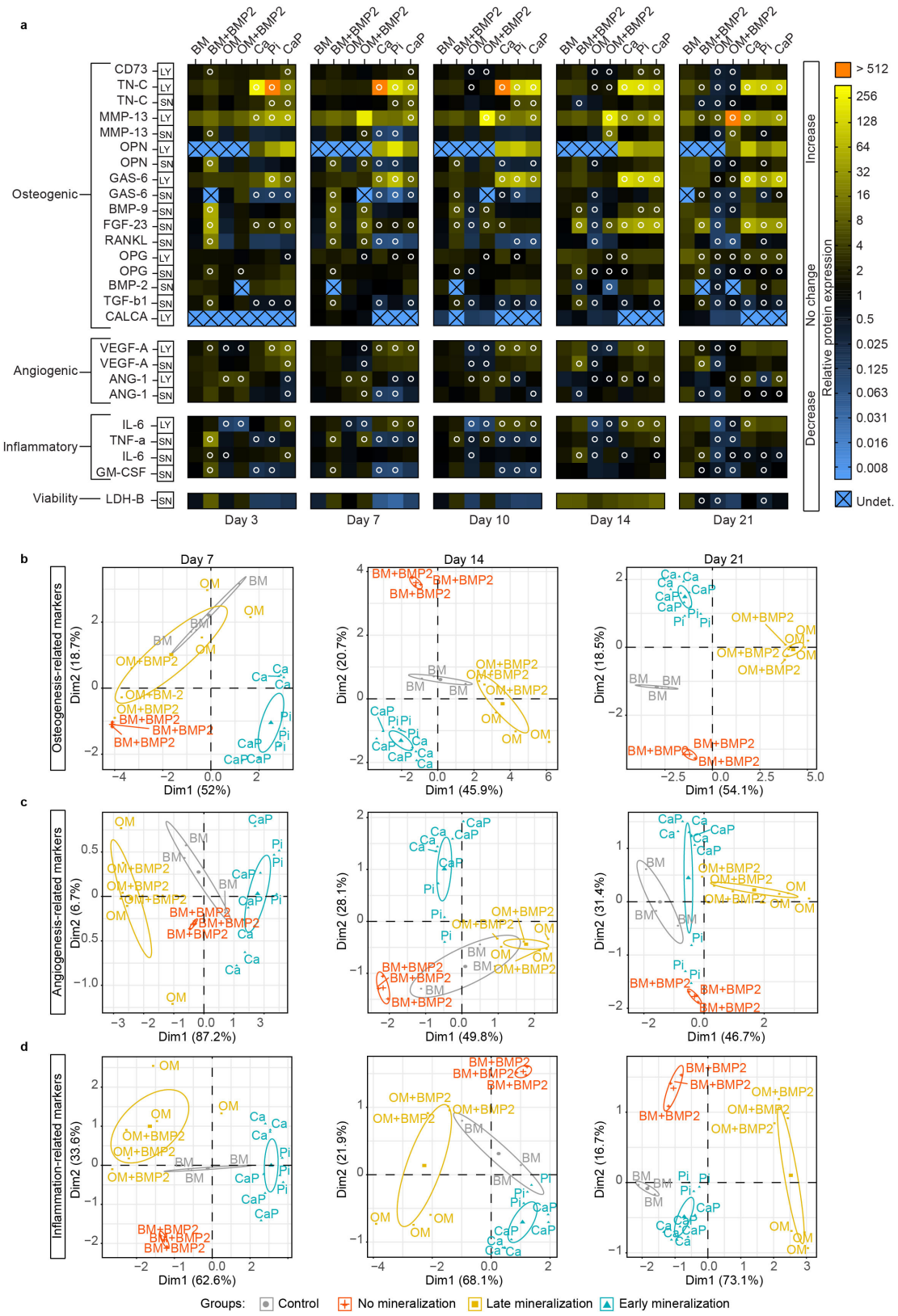

Fig. 4. Multiplex analysis identified differentially expressed proteins as markers for osteogenic differentiation. Protein multiplex analysis of differentiating hMSCs at days 3, 7, 10, 14 and 21 measured in the cell lysate (LY) and supernatant (SN) (**a**) Protein data are represented relative to day 0 expression and normalized to a housekeeping protein (HSP60). Differentially expressed proteins ($p < 0.05$ relative to hMSCs in BM) are indicated with an open white circle. The data represent the mean of three independent experiments (N = 3). "undet": undetected. Principal component analysis was done for all osteogenesis-related protein data (**b**), angiogenesis-related proteins (**c**) and inflammation-related proteins (**d**) at days 7, 14 and 21 (for days 3 and 10, see **Fig. 6**).

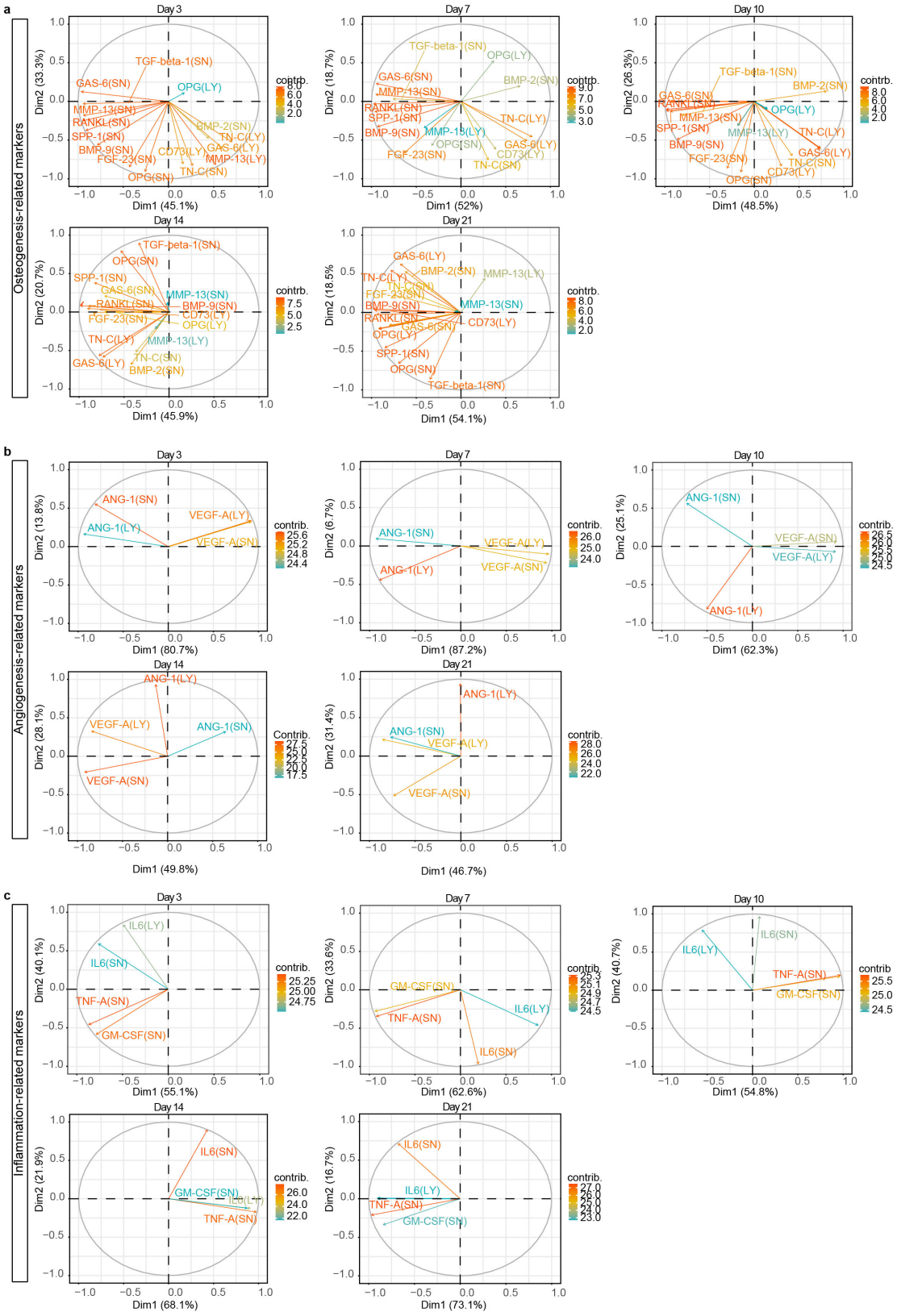

Fig. 5. Principal component analysis (PCA) loading plots showing the contribution of proteins to the principal components. PCA loading plots were generated for osteogenesis-related proteins (**a**), angiogenesis-related proteins (**b**) and inflammation-related proteins (**c**) at days 3, 7, 10, 14 and 21.

both groups were defined by the decrease of TN-C and OPG in the lysate, and GAS-6, RANKL, BMP-9 and FGF-23 in the supernatant. Only one difference was found, which was that MMP-13 in the lysate was decreased in OM and increased in OM+BMP2. A decrease in CD73 was only shown in late-mineralizing hMSCs from day 10 and later time points which may indicate a loss of stemness.

The conditions classified as early-mineralizing demonstrated diversity in their accompanying protein profiles even though they clustered closely beginning on day 7. At day 3, they were similar in their increase of CD73, MMP-13 and GAS-6 in the lysate and their decrease of GAS-6 and TGF-beta-1 in the supernatant. An increase in TN-C in the lysate was found in both hMSCs in Ca and Pi and in the supernatant in Pi and on CaP. At day 7, the early-mineralizing hMSCs were distinguished from non-mineralization hMSCs by their increase in CD73, GAS-6 and MMP-13 in the lysate and their decrease of TGF-beta-1 and GAS-6 in the supernatant. TN-C was increased in the supernatant of hMSCs in Pi and on CaP until day 10. At day 10, the early-mineralizing group was most dissimilar to the other groups, and was marked by an increase in TN-C and GAS-6 in the lysate and a decrease of GAS-6, RANKL, TGF-beta-1, and SPP-1 in the supernatant. It was surprising to see the similarities between the early-mineralizing and the non-mineralizing groups at day 14, where significant differences were only detected in CD73, MMP-13 and GAS-6 in the lysate, all of which were increased in the early-mineralizing group. Ultimately, by day 21, the early-mineralizing group formed a well-defined cluster based on the increase of GAS-6 and TN-C in the lysate and of FGF-23 in the supernatant, and a decrease of OPG in the lysate and of MMP-13, OPG, and TGF-beta-1 in the supernatant, suggesting that we found markers that can distinguish this group, even after mineralization had occurred.

Increased Angiogenesis-Related Marker Expression in Early Mineralizing hMSCs at Multiple Time Points

In addition to osteogenic markers, we determined the protein expression of two angiogenic markers: VEGF-A and ANG-1 (Fig. 4**a**,**c**, Fig. 6**b**). Given we had classified the conditions based on their osteogenic phenotype, it was not surprising that the conditions clustered less closely based on angiogenic markers, but we were nonetheless able to determine informative trends. For example, at day 7, the early-mineralization and late-mineralization groups were clearly different. The late-mineralizing hMSCs expressed higher ANG-1 in the supernatant and lower VEGF-A in both the supernatant and the lysate compared to both the control and the non-mineralization group. Conversely, VEGF-A in the lysate was increased in the early-mineralizing hMSCs and ANG-1 in the supernatant was decreased. This trend continued at day 10, and by day 14, the early-mineralization group had a marked increase in ANG-1 in the lysate compared to the late-mineralization group, suggesting a different differentiation trajectory. After 21 days, the non-mineralization, late-mineralization and early-mineralization hMSCs all had increased ANG-1 in the lysate and decreased ANG-1 in the supernatant.

Inflammation-Related Markers Increased in the Late-Mineralizing hMSCs and Decreased in Late-Mineralizing hMSCs

The protein multiplex assay also contained markers related to the immunomodulatory effect of hMSCs, which is an important process related to bone healing, namely IL-6, TNF-A and GM-CSF (Fig. 4**a**,**d**, Fig. 6**c**). Overall, we found that clustering based on inflammation-related markers was similar to the classification based on mineralization.

Looking first at the non-mineralization hMSCs, which overall clustered closely based on inflammation markers, we found a marked increase in TNF-A and GM-CSF in the supernatant at day 7. By day 14, IL-6 in the supernatant was significantly increased, a trend that continued until day 21. In contrast, the hMSCs classified as late-mineralizing had decreased IL-6 levels in the supernatant at day 3. The different conditions did not cluster closely at days 7 and 10, and by day 14, two different profiles had emerged, both of which had decreased TNF-A in the supernatant, but were distinguished by IL-6 and GM-CSF. Namely, IL-6 was lower in OM than in OM+BMP2, whereas GM-CSF in the supernatant was lower in OM+BMP2 than in OM. The most pronounced difference within the late-mineralization hMSCs cluster was observed at day 21.

The early-mineralization hMSCs had a different profile of inflammatory markers and clustered more closely than the other groups. Until day 7, the inflammatory markers were decreased. Beginning at day 10, IL-6 in the lysate was increased, which continued until day 21. TNF-A in the supernatant was also increased at day 14. At day 21, early-mineralization hMSCs showed a more similar inflammatory profile to control cells in BM than other conditions and were marked by a decrease in IL-6 in the supernatant and an increase in IL-6 in the lysate.

Osteogenic Transcript Expression was Correlated to Mineralization Status

Having evaluated the protein multiplex assay data, we questioned how qRT-PCR of transcripts related to osteogenic differentiation, namely *RUNX2*, *OSX*, *BMP2*, *ALPL*, *SPP1*, *COL1A1* and *SPP1*, would correlate to our findings (Fig. 7). Overall, while there was some correlation to the mineralization classification, the results at the transcript level highlighted the importance of evaluating protein expression.

Non-mineralizing hMSCs did not show an upregulation of any osteogenic genes indicating that no osteogenic differentiation is taking place in these cells. The gene expression profiles of late-mineralizing hMSCs differed from

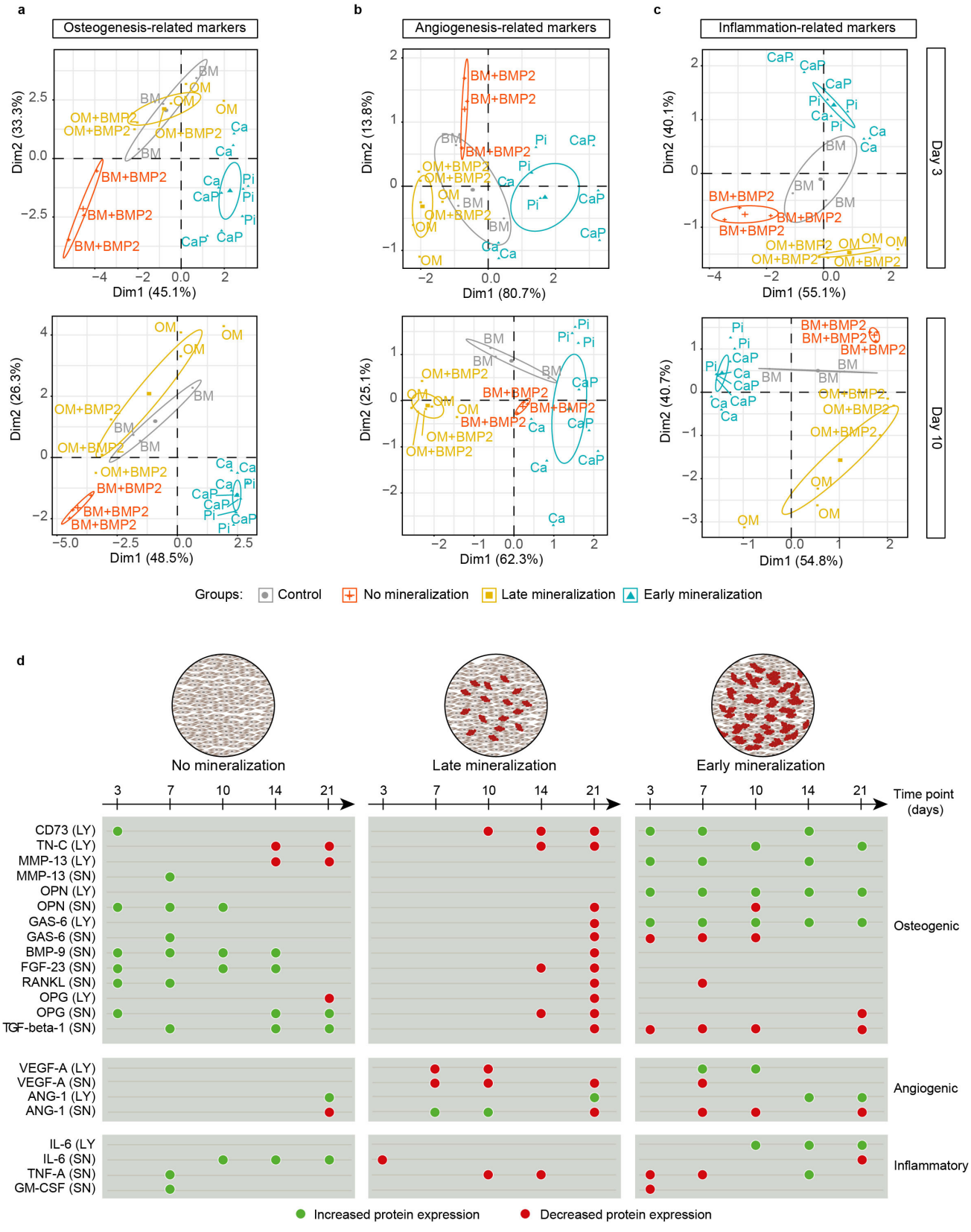

Fig. 6. Principal component analysis and overview of protein expression patterns. PCA was done for osteogenesis-related proteins (**a**), angiogenesis-related proteins (**b**) and inflammation-related proteins (**c**) at days 3 and 10 to show the reproducibility of results. (**d**) Summary of the primary protein expression patterns discussed in this study. Red circles denote decreased protein expression, while green circles signify increased protein expression.

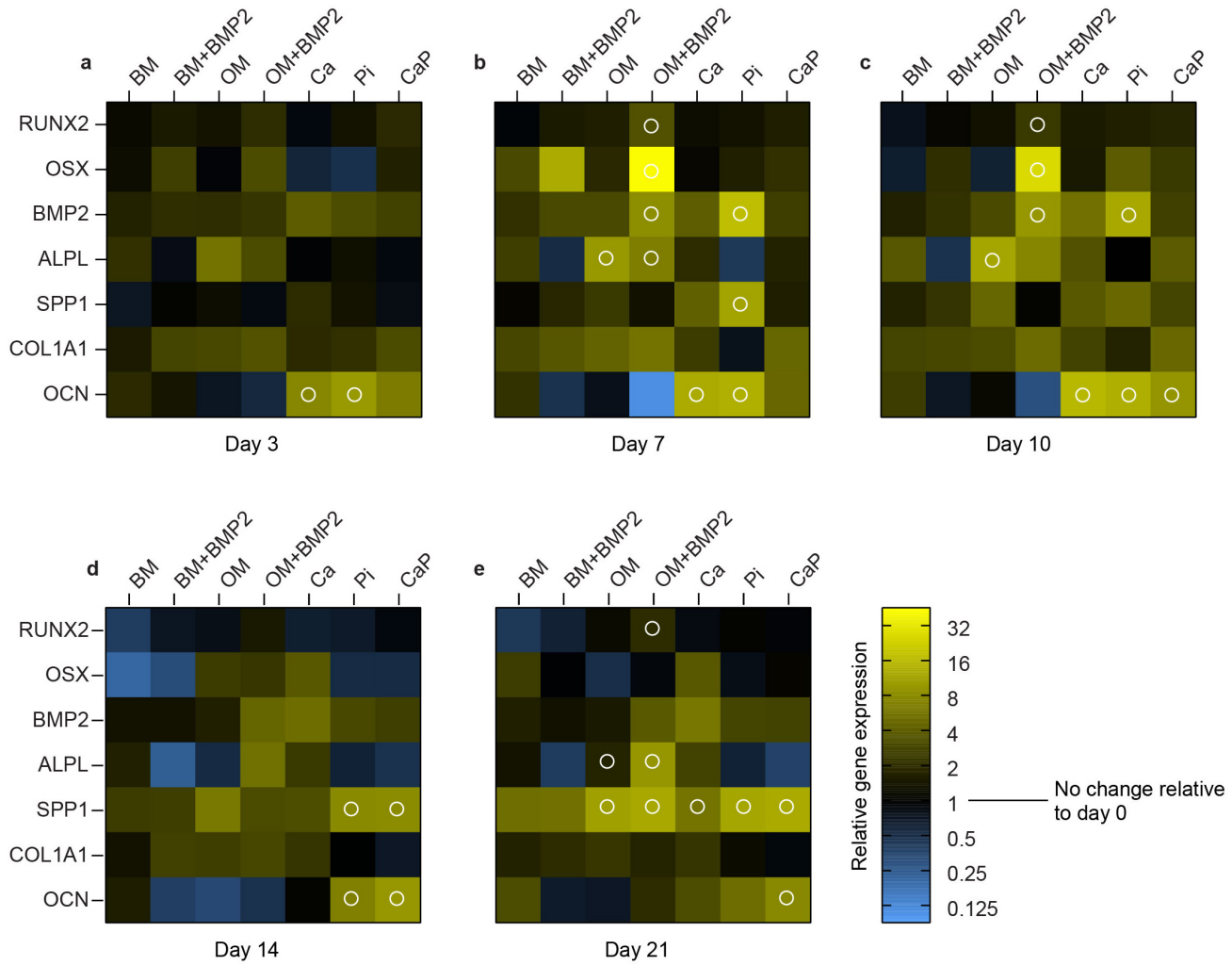

Fig. 7. Osteogenic gene expression over time showed the upregulation of osteogenic markers in late- and early-mineralizing hMSCs. RT-qPCR was done at days 3 (**a**), 7 (**b**), 10 (**c**), 14 (**d**) and 21 (**e**). Ct values were normalized to the geometric mean of two housekeeping proteins (RPLP13A and YWHAZ) and represented relative to a control in BM at day 0. The data represents the mean of three independent experiments (N = 3). Differentially expressed proteins ($p < 0.05$ relative to hMSCs in BM) are indicated with an open white circle.

early-mineralizing hMSCs. For example, an upregulation in *RUNX-2* and *OSX*, both transcription factors in osteogenesis, was detected at early time points in late-mineralizing hMSCs (days 7 and 10), as well as *ALPL* and *BMP2* expression. In comparison, early-mineralizing hMSCs showed an upregulation of *OCN* early on and maintained this until later time points (days 3 until 21). *SPP1* expression was upregulated in both mineralizing groups at a later time point. However, when comparing gene expression results with the protein multiplex analysis, differences between conditions and mineralization status were detected more clearly on the protein level, confirming that a qPCR is a less powerful assay to characterize differentiation.

Discussion

Inducing osteogenic differentiation in hMSCs has been achieved through multiple approaches, especially by the addition of pro-osteogenic factors to achieve an osteoblast-like phenotype and the secretion of a mineralized extracellular matrix. Unfortunately, there has been a poor correlation between *in vitro* and *in vivo* work, suggesting a need to improve how osteogenic differentiation is achieved and investigated *in vitro*. *In vitro* differentiation models oftentimes are evaluated using limited readouts to assess osteogenic differentiation, whereas a broader range of markers could offer better insight. Therefore, in this study, we propose a protein multiplex assay to evaluate the phenotype of hMSCs undergoing osteogenic differentiation. We set up a targeted 18-plex protein panel of markers for osteogenesis, angiogenesis, or inflammation in order to characterize different strategies of inducing osteogenic differentiation in hMSCs, to identify relevant patterns, and to gain a better understanding of osteogenic differentiation *in vitro*. HMSCs were stimulated with a combination of dexamethasone,

β-glycerophosphate and ascorbic acid (OM), with growth factors such as BMP-2 (BM+BMP2 and OM+BMP2) or by supplementing calcium (Ca) or phosphate ions (Pi) or by seeding on a CaP-based biomaterial (CaP), all conditions that have previously been shown to induce osteogenic differentiation.

Mineral deposition, as measured by ARS was used for the classification of these conditions. It is important to note that, in the context of our measurements, we cannot rule out the possibility that some calcium deposition observed may be attributed to the release of calcium upon cell death, which could have contributed to the overall mineralization measurement. Protein patterns were associated with different experimental groups classified as inducers of non- (BM and BM+BMP2), late- (OM and OM+BMP2) and early- (Ca, Pi and CaP) mineralization. It was interesting to note that differences were also found within the mineralization groups, which speaks to the complexity of assessing osteogenic differentiation. For example, many differences in the osteogenic protein profiles between hMSCs in OM and OM+BMP2 were detected until day 14, even though their mineralization status was similar. Their protein profiles related to inflammation and angiogenesis were, however, much more similar. Overall, while osteogenic markers varied substantially within mineralization classifications, the angiogenic and inflammatory markers were more similar according to mineralization status.

No significant difference in LDH-B protein release as compared to the control in BM was detected (Fig. 3**a**), suggesting the absence of cytotoxicity. This is further supported by the phase contrast images obtained during the culture period (Fig. 1**b**,**c**). However, to provide a definitive confirmation of cell viability, it is advisable to conduct additional assays such as an MTT assay.

The protein panel contained nine markers selected to characterize osteogenic differentiation in hMSCs: BMP-2, BMP-9, GAS-6, FGF-23, TGF-beta-1, RANKL, OPG, SPP-1 and MMP-13. Two of the markers tested, BMP-9 and FGF-23, failed to distinguish the differences we observed in the mineralization status between groups. However, our results indicate that the increased expression of these two markers may be linked to the supplementation of BMP-2 to the medium, which was sufficient to stimulate BMP-9 and FGF-23 at early time points (day 3 until 10) in hMSCs in both BM+BMP2 and OM+BMP2, but was insufficient to promote an osteoblastic phenotype.

In contrast, TGF-beta-1 in the supernatant emerged as an interesting factor to correlate to mineral deposition: Its decrease was detected in late- (OM) and early- (Ca, Pi and CaP) mineralizing hMSCs. TGF-beta-1 plays a crucial role in chondrogenesis and bone formation and resorption (Zhao and Hantash, 2011). It promotes osteoprogenitor proliferation and early differentiation, but also inhibits mineralization in the late stage of osteoblast differentiation have shown that TGF-beta-1 supplementation to hMSCs can decrease their mineralization (Cals *et al.*, 2012; Nam *et al.*, 2020), which is in line with our results. While there are also studies that state the opposite, it is widely accepted that TGF-beta-1 has a broad range of effects on bone metabolism and its level in the supernatant could prove to be a useful predictor of osteogenic differentiation (Jilka *et al.*, 1998; Kasagi and Chen, 2013; Kassem *et al.*, 2000; Pfeilschifter *et al.*, 1990).

We also found two markers, GAS-6 and MMP-13, indicative of osteogenic differentiation, but with different expression patterns in the supernatant and the lysate, underlining the power of this particular assay. First, we found GAS-6 to be an indicative marker for early-mineralizing hMSCs. GAS-6 has previously been reported in osteoblasts to have a stimulatory effect on bone resorption by osteoclasts (Nakamura *et al*., 1998; Shiozawa *et al*., 2010). Its expression in the supernatant in the non-mineralizing hMSCs (BM+BMP2) was increased, whereas its expression in the lysate was decreased. The opposite was true for the early-mineralizing hMSCs (Ca, Pi and CaP). This indicates that GAS-6 may not be released or may remain in the extracellular matrix. Second, MMP-13 in the supernatant was found in conditions lacking mineralization, whereas MMP-13 in the lysate was found in mineralizing hMSCs. MMP-13 in the native bone ECM plays a role in bone remodeling and is a key enzyme for collagen type 1 degradation (Wu *et al.*, 2002). Our results indicate that MMP-13 could be successfully correlated to the differentiated phenotype marked by mineral deposition.

Because we were introducing a novel approach to characterize differentiation in hMSCs, we also wanted to use conventional methodology. ALP activity was therefore quantified as an important enzyme involved in mineral deposition in bone remodeling (Hessle *et al.*, 2002). ALP activity directly correlated to mineralization for late-mineralizing hMSCs, but was inversely correlated to mineralization status in early-mineralizing hMSCs. While the upregulation of ALP activity in late-mineralizing hMSCs has been previously explained by the supplementation of dexamethasone in the medium (Wong *et al.*, 1990), it could be that the early upregulation of ALP activity reduced inorganic pyrophosphate, a hydroxyapatite-forming blocker, and supplied inorganic phosphate for hydroxyapatite production (Whyte *et al.*, 1995). These findings may be explained by the known downregulation of ALP caused by high concentrations of phosphate (Liu *et al.*, 2009), or the upregulation known to be caused by BMP-2 supplementation (Vanhatupa *et al.*, 2015).Together, this shows that investigating ALP activity alone is insufficient to determine whether hMSCs are undergoing osteogenic differentiation.

A correlation between the transcript expression of osteogenic markers and the mineralization state of hMSCs was only found for *SPP1*, the gene coding for Osteopontin that is commonly expressed in osteoblasts, at a late time point (day 21) as it was upregulated in all conditions that

were able to mineralize. The differences in relative gene expression levels were not as pronounced as the variations observed at the protein level. *OCN*, which is involved in matrix mineralization by binding hydroxyapatite, as well as *SPP1* were upregulated in early-mineralizing hMSCs at several time points (Danoux *et al.*, 2015; Tsao *et al.*, 2017). No differences in any gene expression profiles were found between hMSCs in BM and BM+BMP2. Even though the supplementation of BMP-2 activated certain pathways, the concentration used here, 50 ng/mL, was insufficient to induce osteogenic differentiation in hMSCs on its own. In hMSCs in OM+BMP2, however, the supplementation seemed to enhance osteogenesis in comparison with hMSCs in OM, which has been previously reported (Vanhatupa *et al.*, 2015).

Angiogenic protein marker expression did not correlate to mineralization status of hMSCs but it was similar within mineralization groups, possibly due to the limitations of the *in vitro* model used in this study. The use of hMSCs in 2D does not recapitulate the complexities of the angiogenic processes *in vivo* (Liang *et al*., 2017). However, it can indicate whether the differentiating hMSCs release angiogenic factors which potentially will stimulate angiogenesis in surrounding cells. Here, we measured the expression of VEGF-A and ANG-1, which promote angiogenesis and immunomodulatory functions, and have been shown to improve bone formation (Rundle *et al.*, 2006; Shin *et al.*, 2021). Non-mineralization hMSCs had increased VEGF-A in the supernatant and showed an increase in VEGF-A over time, indicating a pro-angiogenic effect in agreement with previous reports (Krawiec *et al.*, 2015). Furthermore, the increase in TGF-beta-1, which besides being an osteogenesis-related marker is also considered an angiogenic factor that directly targets VEGF-A, supports this claim (Sánchez-Elsner *et al.*, 2001). Late-mineralization hMSCs showed an opposing trend in angiogenic factors than early-mineralization hMSCs at early time points, with an increase in ANG-1 and a decrease of VEGF-A. Hoch *et al*. (2012) attributed this to the dexamethasone-containing differentiation medium and concluded that differentiated MSCs have diminished angiogenic potential (Hoch *et al.*, 2012). However, we found that hMSCs classified as early-mineralizing maintained their angiogenic potential with an initial increase of VEGF-A.

Inflammation plays an important role in bone healing (Kon *et al.*, 2001; Rundle *et al.*, 2006), and hMSCs are known to secrete immunomodulatory factors such as IL-6, TNF-A or GM-CSF (Shin *et al.*, 2021). The non-mineralizing hMSCs (BM+BMP2) expressed higher IL-6 in the supernatant, suggesting a positive effect on bone healing. IL-6 is a pro-inflammatory cytokine shown to influence the MAPK signaling cascade, which is an essential process for bone formation. It is, however, also correlated with the severity of inflammation (De Benedetti *et al.*, 2006). High IL-6 in the supernatant was also seen in the early-mineralizing group, but not in the late-mineralizing group, which had diminished IL-6 in the lysate in agreement with previous studies (Pricola *et al.*, 2009). Early-mineralizing hMSCs had diminished TNF-A, an inflammatory factor shown to stimulate osteoclast-induced bone resorption with a described inhibitory effect on osteogenic differentiation at high concentrations (Zhao *et al.*, 2011), as well as GM-CSF, a cytokine related to bone resorption that regulates the fusion of mononuclear osteoclasts into bone-resorbing osteoclasts (Lee *et al.*, 2009). Combined with the finding on IL-6, which may result in suppression of neutrophil apoptosis, favoring M2 polarization in macrophages *in vivo*, it could be that these hMSCs could participate in a healing process (Philipp *et al.*, 2018; Raffaghello *et al.*, 2008). Bastidas-Coral *et al*. (2016) have shown an increased induction of mineralization in hMSCs stimulated with IL-6 (Bastidas-Coral *et al.*, 2016). Therefore, increased IL-6 expression in early-mineralizing hMSCs may also be connected to the increased mineral deposition.

Conclusion

In summary, it was shown that early- and late-mineralizing hMSCs undergo osteogenic differentiation, albeit with a difference in the way this is taking place. Non-mineralizing hMSCs in BM+BMP2 did not undergo osteogenic differentiation in our experiments, however, a beneficial effect on angiogenesis and inflammation markers was detected, both relevant for the bone healing process. While late-mineralizing hMSCs in OM and OM+BMP2 had minimal potential to secrete angiogeneic factors, early-mineralizing hMSCs did show an increased effect. Both non- and early-mineralizing hMSCs showed expression of markers related to inflammation. TGF-beta-1 was identified as an interesting marker inversely correlating to mineral deposition. GAS-6 as well as MMP-13 expression were highlighted as markers indicative of osteogenic differentiation. A comprehensive roadmap of osteogenic differentiation was established, and potential markers of interest were highlighted. A targeted proteomic screening approach such as a protein multiplex assay could be an improvement of how osteogenic differentiation is analyzed *in vitro* and be a first step to improve the poor correlation between *in vitro* and *in vivo* results (Hulsart-Billström *et al.*, 2016). This approach may potentially improve the *in vitro* evaluation of biomaterials for bone regeneration, as has been shown here on the example of hMSCs on a CaP coating. In future research, building on these results, it would be interesting to transition to a 3D model which could further enhance the translational capacity of our findings. Overall, we were able to compare different commonly used *in vitro* models of osteogenic differentiation in hMSCs, giving a side-by-side comparison that has been lacking.

List of Abbreviations

hMSCs, human mesenchymal stem cells; 3D, three-dimensional; 2D, two-dimensional; ALP, alkaline phosphatase; BMP2, bone morphogenetic protein-2; BMP7, bone morphogenetic protein-7; BMP9, bone morphogenetic protein-9; TGF-beta-1, transforming growth factor beta-1; Ca, calcium; Pi, phosphate ions; CaP, calcium phosphate; ARS, Alizarin red S; MMP-13, matrix metalloproteinase-13; GAS-6, growth arrest-specific 6; CO_2, carbon dioxide; BM, basic medium; ATR-FTIR, Attenuated total reflectance Fourier-transform infrared spectroscopy; OM, osteogenic medium; FGF-23, fibroblast growth factor-23; OPG, osteoprotegerin; RANKL, receptor activator of NF-κB ligand; GAS-6, growth arrest-specific protein 6; TN-C, tenascin-C; ANG-1, angiopoietin-1; VEGF-A, vascular endothelial growth factor A; IL-6, interleukin-6; GM-CSF, granulocyte-macrophage colony-stimulating factor; LDH-B, L-lactate dehydrogenase B; PBS, phosphate buffered saline; *RUNX2*, runt-related transcription factor 2; *OSX*, osterix; *COL1A1*, collagen type I alpha 1 chain; *OCN*, osteocalcin; ANOVA, analysis of variance; PCA, principal component analysis; LY, lysates; SN, supernatants; XRD, X-Ray Diffraction; SEM, Scanning Electron Microscopy; EDS, Energy-Dispersive X-Ray Spectroscopy.

Availability of Data and Materials

The data will be made available upon request.

Author Contributions

MEL: Investigation, conceptualization, methodology, formal analysis, writing – original draft preparation. ZTB: conceptualization, writing - review and editing. YAS: Investigation, visualization. LE: Software, formal analysis. HR: writing - review and editing, conceptualization and design of work. MS: Supervision, conceptualization. MvG: Supervision, conceptualization. VLP: Supervision, conceptualization, writing - review and editing. PH: supervision, conceptualization, writing - review and editing, and funding acquisition. All authors contributed to editorial changes in the manuscript, read and approved the final manuscript, and have participated sufficiently in the work to take public responsibility for appropriate portions of the content. All authors have agreed to be accountable for all aspects of the work.

Ethics Approval and Consent to Participate

Not applicable.

Acknowledgments

The authors would like to thank Frederik Jan van Schooten, Geja Hageman, Sven Rouschop and Wenbo Wu at the Department of Pharmacology and Toxicology (Maastricht University) for allowing us to use their Luminex 100 instrument and for the assistance provided with the multiplex assay, as well as Jarno Koetsier at the Faculty of Science and Engineering (Maastricht University) for assisting with the multiplex data analysis. We're grateful to Hang Nguyen for critically reading this manuscript and offering her input.

Funding

This research has been made possible with the support of the Dutch Research Council (NWO) Talent Program – Vidi (Bone Microfactory project, No. 15604), the Dutch Province of Limburg (LINK project) and the Interreg Vlaanderen/ Nederland project 'BIOMAT-on-microfluidic-chip'. PH gratefully acknowledges the NWO Gravitation Program 'Materials-Driven Regeneration', funded by the Netherlands Organization for Scientific Research (024.003.013).

Conflict of Interest

The authors declare no conflict of interest.

References

Alves H, Dechering K, Van Blitterswijk C, De Boer J (2011) High-throughput assay for the identification of compounds regulating osteogenic differentiation of human mesenchymal stromal cells. PloS One 6: e26678. DOI: 10.1371/journal.pone.0026678.

Aquino-Martínez R, Artigas N, Gámez B, Rosa JL, Ventura F (2017) Extracellular calcium promotes bone formation from bone marrow mesenchymal stem cells by amplifying the effects of BMP-2 on SMAD signalling. PloS One 12: e0178158. DOI: 10.1371/journal.pone.0178158.

Bastidas-Coral AP, Bakker AD, Zandieh-Doulabi B, Kleverlaan CJ, Bravenboer N, Forouzanfar T, Klein-Nulend J (2016) Cytokines TNF-α, IL-6, IL-17F, and IL-4 Differentially Affect Osteogenic Differentiation of Human Adipose Stem Cells. Stem Cells International 2016: 1318256. DOI: 10.1155/2016/1318256.

Bhat S, Viswanathan P, Chandanala S, Prasanna SJ, Seetharam RN (2021) Expansion and characterization of bone marrow derived human mesenchymal stromal cells in serum-free conditions. Scientific Reports 11: 3403. DOI: 10.1038/s41598-021-83088-1.

Braccini A, Wendt D, Jaquiery C, Jakob M, Heberer M, Kenins L, Wodnar-Filipowicz A, Quarto R, Martin I (2005) Three-dimensional perfusion culture of human bone marrow cells and generation of osteoinductive grafts. Stem Cells (Dayton, Ohio) 23: 1066-1072. DOI: 10.1634/stemcells.2005-0002.

Calori GM, Mazza E, Colombo M, Ripamonti C (2011) The use of bone-graft substitutes in large bone defects: any specific needs? Injury 42 2: S56-S63. DOI: 10.1016/j.injury.2011.06.011.

Cals FLJ, Hellingman CA, Koevoet W, Baatenburg de

Jong RJ, van Osch GJVM (2012) Effects of transforming growth factor-β subtypes on in vitro cartilage production and mineralization of human bone marrow stromal-derived mesenchymal stem cells. Journal of Tissue Engineering and Regenerative Medicine 6: 68-76. DOI: 10.1002/term.399.

Clark AY, Martin KE, García JR, Johnson CT, Theriault HS, Han WM, Zhou DW, Botchwey EA, García AJ (2020) Integrin-specific hydrogels modulate transplanted human bone marrow-derived mesenchymal stem cell survival, engraftment, and reparative activities. Nature Communications 11: 114. DOI: 10.1038/s41467-019-14000-9.

Danoux CBSS, Bassett DC, Othman Z, Rodrigues AI, Reis RL, Barralet JE, van Blitterswijk CA, Habibovic P (2015) Elucidating the individual effects of calcium and phosphate ions on hMSCs by using composite materials. Acta Biomaterialia 17: 1-15. DOI: 10.1016/j.actbio.2015.02.003.

De Benedetti F, Rucci N, Del Fattore A, Peruzzi B, Paro R, Longo M, Vivarelli M, Muratori F, Berni S, Ballanti P, Ferrari S, Teti A (2006) Impaired skeletal development in interleukin-6-transgenic mice: a model for the impact of chronic inflammation on the growing skeletal system. Arthritis and Rheumatism 54: 3551-3563. DOI: 10.1002/art.22175.

Doebelin N, Kleeberg R (2015) Profex: a graphical user interface for the Rietveld refinement program BGMN. Journal of Applied Crystallography 48: 1573-1580. DOI: 10.1107/S1600576715014685.

Fischer M, Schoon J, Freund E, Miebach L, Weltmann KD, Bekeschus S, Wassilew GI (2022) Biocompatible Gas Plasma Treatment Affects Secretion Profiles but Not Osteogenic Differentiation in Patient-Derived Mesenchymal Stromal Cells. International Journal of Molecular Sciences 23: 2038. DOI: 10.3390/ijms23042038.

Han SH, Cha M, Jin YZ, Lee KM, Lee JH (2020) BMP-2 and hMSC dual delivery onto 3D printed PLA-Biogel scaffold for critical-size bone defect regeneration in rabbit tibia. Biomedical Materials (Bristol, England) 16: 015019. DOI: 10.1088/1748-605X/aba879.

Herberg S, Varghai D, Alt DS, Dang PN, Park H, Cheng Y, Shin JY, Dikina AD, Boerckel JD, Rolle MW, Alsberg E (2021) Scaffold-free human mesenchymal stem cell construct geometry regulates long bone regeneration. Communications Biology 4: 89. DOI: 10.1038/s42003-020-01576-y.

Hessle L, Johnson KA, Anderson HC, Narisawa S, Sali A, Goding JW, Terkeltaub R, Millan JL (2002) Tissue-nonspecific alkaline phosphatase and plasma cell membrane glycoprotein-1 are central antagonistic regulators of bone mineralization. Proceedings of the National Academy of Sciences of the United States of America 99: 9445-9449. DOI: 10.1073/pnas.142063399.

Hoch AI, Binder BY, Genetos DC, Leach JK (2012) Differentiation-dependent secretion of proangiogenic factors by mesenchymal stem cells. PloS One 7: e35579. DOI: 10.1371/journal.pone.0035579.

Hulsart-Billström G, Dawson JI, Hofmann S, Müller R, Stoddart MJ, Alini M, Redl H, El Haj A, Brown R, Salih V, Hilborn J, Larsson S, Oreffo RO (2016) A surprisingly poor correlation between in vitro and in vivo testing of biomaterials for bone regeneration: results of a multicentre analysis. European Cells & Materials 31: 312-322. DOI: 10.22203/ecm.v031a20.

Jilka RL, Weinstein RS, Bellido T, Parfitt AM, Manolagas SC (1998) Osteoblast programmed cell death (apoptosis): modulation by growth factors and cytokines. Journal of Bone and Mineral Research: the Official Journal of the American Society for Bone and Mineral Research 13: 793-802. DOI: 10.1359/jbmr.1998.13.5.793.

Kasagi S, Chen W (2013) TGF-beta1 on osteoimmunology and the bone component cells. Cell & Bioscience 3: 4. DOI: 10.1186/2045-3701-3-4.

Kassem M, Kveiborg M, Eriksen EF (2000) Production and action of transforming growth factor-beta in human osteoblast cultures: dependence on cell differentiation and modulation by calcitriol. European Journal of Clinical Investigation 30: 429-437. DOI: 10.1046/j.1365-2362.2000.00645.x.

Kehl D, Generali M, Mallone A, Heller M, Uldry AC, Cheng P, Gantenbein B, Hoerstrup SP, Weber B (2019) Proteomic analysis of human mesenchymal stromal cell secretomes: a systematic comparison of the angiogenic potential. NPJ Regenerative Medicine 4: 8. DOI: 10.1038/s41536-019-0070-y.

Kon T, Cho TJ, Aizawa T, Yamazaki M, Nooh N, Graves D, Gerstenfeld LC, Einhorn TA (2001) Expression of osteoprotegerin, receptor activator of NF-kappaB ligand (osteoprotegerin ligand) and related proinflammatory cytokines during fracture healing. Journal of Bone and Mineral Research: the Official Journal of the American Society for Bone and Mineral Research 16: 1004-1014. DOI: 10.1359/jbmr.2001.16.6.1004.

Krawiec JT, Weinbaum JS, St Croix CM, Phillippi JA, Watkins SC, Rubin JP, Vorp DA (2015) A cautionary tale for autologous vascular tissue engineering: impact of human demographics on the ability of adipose-derived mesenchymal stem cells to recruit and differentiate into smooth muscle cells. Tissue Engineering. Part a 21: 426-437. DOI: 10.1089/ten.TEA.2014.0208.

Lee MN, Hwang HS, Oh SH, Roshanzadeh A, Kim JW, Song JH, Kim ES, Koh JT (2018) Elevated extracellular calcium ions promote proliferation and migration of mesenchymal stem cells via increasing osteopontin expression. Experimental & Molecular Medicine 50: 1-16. DOI: 10.1038/s12276-018-0170-6.

Lee MS, Kim HS, Yeon JT, Choi SW, Chun CH, Kwak HB, Oh J (2009) GM-CSF regulates fusion of mononuclear osteoclasts into bone-resorbing osteoclasts by activating the Ras/ERK pathway. Journal of Immunology (Baltimore, Md.: 1950) 183: 3390-3399. DOI: 10.4049/jim-

munol.0804314.

Lei Q, Chen J, Huang W, Wu D, Lin H, Lai Y (2015) Proteomic analysis of the effect of extracellular calcium ions on human mesenchymal stem cells: Implications for bone tissue engineering. Chemico-biological Interactions 233: 139-146. DOI: 10.1016/j.cbi.2015.03.021.

Liang T, Zhu L, Gao W, Gong M, Ren J, Yao H, Wang K, Shi D (2017) Coculture of endothelial progenitor cells and mesenchymal stem cells enhanced their proliferation and angiogenesis through PDGF and Notch signaling. FEBS Open Bio 7: 1722-1736. DOI: 10.1002/2211-5463.12317.

Liu YK, Lu QZ, Pei R, Ji HJ, Zhou GS, Zhao XL, Tang RK, Zhang M (2009) The effect of extracellular calcium and inorganic phosphate on the growth and osteogenic differentiation of mesenchymal stem cells in vitro: implication for bone tissue engineering. Biomedical Materials (Bristol, England) 4: 025004. DOI: 10.1088/1748-6041/4/2/025004.

McCullen SD, Zhan J, Onorato ML, Bernacki SH, Loboa EG (2010) Effect of varied ionic calcium on human adipose-derived stem cell mineralization. Tissue Engineering. Part a 16: 1971-1981. DOI: 10.1089/ten.TEA.2009.0691.

Nakamura YS, Hakeda Y, Takakura N, Kameda T, Hamaguchi I, Miyamoto T, Kakudo S, Nakano T, Kumegawa M, Suda T (1998) Tyro 3 receptor tyrosine kinase and its ligand, Gas6, stimulate the function of osteoclasts. Stem Cells (Dayton, Ohio) 16: 229-238. DOI: 10.1002/stem.160229.

Nam B, Park H, Lee YL, Oh Y, Park J, Kim SY, Weon S, Choi SH, Yang JH, Jo S, Kim TH (2020) TGFβ1 Suppressed Matrix Mineralization of Osteoblasts Differentiation by Regulating SMURF1-C/EBPβ-DKK1 Axis. International Journal of Molecular Sciences 21: 9771. DOI: 10.3390/ijms21249771.

Pfeilschifter J, Wolf O, Naumann A, Minne HW, Mundy GR, Ziegler R (1990) Chemotactic response of osteoblastlike cells to transforming growth factor beta. Journal of Bone and Mineral Research: the Official Journal of the American Society for Bone and Mineral Research 5: 825-830. DOI: 10.1002/jbmr.5650050805.

Philipp D, Suhr L, Wahlers T, Choi YH, Paunel-Görgülü A (2018) Preconditioning of bone marrow-derived mesenchymal stem cells highly strengthens their potential to promote IL-6-dependent M2b polarization. Stem Cell Research & Therapy 9: 286. DOI: 10.1186/s13287-018-1039-2.

Pricola KL, Kuhn NZ, Haleem-Smith H, Song Y, Tuan RS (2009) Interleukin-6 maintains bone marrow-derived mesenchymal stem cell stemness by an ERK1/2-dependent mechanism. Journal of Cellular Biochemistry 108: 577-588. DOI: 10.1002/jcb.22289.

Quade M, Münch P, Lode A, Duin S, Vater C, Gabrielyan A, Rösen-Wolff A, Gelinsky M (2020) The Secretome of Hypoxia Conditioned hMSC Loaded in a Central Depot Induces Chemotaxis and Angiogenesis in a Biomimetic Mineralized Collagen Bone Replacement Material. Advanced Healthcare Materials 9: e1901426. DOI: 10.1002/adhm.201901426.

Raffaghello L, Bianchi G, Bertolotto M, Montecucco F, Busca A, Dallegri F, Ottonello L, Pistoia V (2008) Human mesenchymal stem cells inhibit neutrophil apoptosis: a model for neutrophil preservation in the bone marrow niche. Stem Cells (Dayton, Ohio) 26: 151-162. DOI: 10.1634/stemcells.2007-0416.

Rundle CH, Wang H, Yu H, Chadwick RB, Davis EI, Wergedal JE, Lau KHW, Mohan S, Ryaby JT, Baylink DJ (2006) Microarray analysis of gene expression during the inflammation and endochondral bone formation stages of rat femur fracture repair. Bone 38: 521-529. DOI: 10.1016/j.bone.2005.09.015.

Sánchez-Elsner T, Botella LM, Velasco B, Corbí A, Attisano L, Bernabéu C (2001) Synergistic cooperation between hypoxia and transforming growth factor-beta pathways on human vascular endothelial growth factor gene expression. The Journal of Biological Chemistry 276: 38527-38535. DOI: 10.1074/jbc.M104536200.

Sha J, Kanno T, Miyamoto K, Bai Y, Hideshima K, Matsuzaki Y (2019) Application of a Bioactive/Bioresorbable Three-Dimensional Porous Uncalcined and Unsintered Hydroxyapatite/Poly-D/L-lactide Composite with Human Mesenchymal Stem Cells for Bone Regeneration in Maxillofacial Surgery: A Pilot Animal Study. Materials (Basel, Switzerland) 12: 705. DOI: 10.3390/ma12050705.

Shin S, Lee J, Kwon Y, Park KS, Jeong JH, Choi SJ, Bang SI, Chang JW, Lee C (2021) Comparative Proteomic Analysis of the Mesenchymal Stem Cells Secretome from Adipose, Bone Marrow, Placenta and Wharton's Jelly. International Journal of Molecular Sciences 22: 845. DOI: 10.3390/ijms22020845.

Shiozawa Y, Pedersen EA, Patel LR, Ziegler AM, Havens AM, Jung Y, Wang J, Zalucha S, Loberg RD, Pienta KJ, Taichman RS (2010) GAS6/AXL axis regulates prostate cancer invasion, proliferation, and survival in the bone marrow niche. Neoplasia (New York, N.Y.) 12: 116-127. DOI: 10.1593/neo.91384.

Sordi MB, Curtarelli RB, da Silva IT, Fongaro G, Benfatti CAM, de Souza Magini R, Cabral da Cruz AC (2021) Effect of dexamethasone as osteogenic supplementation in in vitro osteogenic differentiation of stem cells from human exfoliated deciduous teeth. Journal of Materials Science. Materials in Medicine 32: 1. DOI: 10.1007/s10856-020-06475-6.

Taylor B, Indano S, Yankannah Y, Patel P, Perez XI, Freeman J (2019) Decellularized Cortical Bone Scaffold Promotes Organized Neovascularization In Vivo. Tissue Engineering. Part a 25: 964-977. DOI: 10.1089/ten.TEA.2018.0225.

Tsao YT, Huang YJ, Wu HH, Liu YA, Liu YS, Lee OK (2017) Osteocalcin Mediates Biomineralization during Osteogenic Maturation in Human Mesenchymal Stromal Cells. International Journal of Molecular Sciences 18: 159. DOI: 10.3390/ijms18010159.

Vanhatupa S, Ojansivu M, Autio R, Juntunen M, Miettinen S (2015) Bone Morphogenetic Protein-2 Induces Donor-Dependent Osteogenic and Adipogenic Differentiation in Human Adipose Stem Cells. Stem Cells Translational Medicine 4: 1391-1402. DOI: 10.5966/sctm.2015-0042.

Whyte MP, Landt M, Ryan LM, Mulivor RA, Henthorn PS, Fedde KN, Mahuren JD, Coburn SP (1995) Alkaline phosphatase: placental and tissue-nonspecific isoenzymes hydrolyze phosphoethanolamine, inorganic pyrophosphate, and pyridoxal 5'-phosphate. Substrate accumulation in carriers of hypophosphatasia corrects during pregnancy. The Journal of Clinical Investigation 95: 1440-1445. DOI: 10.1172/JCI117814.

Wong MM, Rao LG, Ly H, Hamilton L, Tong J, Sturtridge W, McBroom R, Aubin JE, Murray TM (1990) Long-term effects of physiologic concentrations of dexamethasone on human bone-derived cells. Journal of Bone and Mineral Research: the Official Journal of the American Society for Bone and Mineral Research 5: 803-813. DOI: 10.1002/jbmr.5650050803.

Wu N, Opalenik S, Liu J, Jansen ED, Giro MG, Davidson JM (2002) Real-time visualization of MMP-13 promoter activity in transgenic mice. Matrix Biology: Journal of the International Society for Matrix Biology 21: 149-161. DOI: 10.1016/s0945-053x(01)00192-5.

Xu J, Liu J, Gan Y, Dai K, Zhao J, Huang M, Huang Y, Zhuang Y, Zhang X (2020) High-Dose TGF-β1 Impairs Mesenchymal Stem Cell-Mediated Bone Regeneration via Bmp2 Inhibition. Journal of Bone and Mineral Research: the Official Journal of the American Society for Bone and Mineral Research 35: 167-180. DOI: 10.1002/jbmr.3871.

Xu L, Liu Y, Sun Y, Wang B, Xiong Y, Lin W, Wei Q, Wang H, He W, Wang B, Li G (2017) Tissue source determines the differentiation potentials of mesenchymal stem cells: a comparative study of human mesenchymal stem cells from bone marrow and adipose tissue. Stem Cell Research & Therapy 8: 275. DOI: 10.1186/s13287-017-0716-x.

Yang L, Hedhammar M, Blom T, Leifer K, Johansson J, Habibovic P, van Blitterswijk CA (2010) Biomimetic calcium phosphate coatings on recombinant spider silk fibres. Biomedical Materials (Bristol, England) 5: 045002. DOI: 10.1088/1748-6041/5/4/045002.

Yang Y, Luo Z, Zhao Y (2018) Osteostimulation scaffolds of stem cells: BMP-7-derived peptide-decorated alginate porous scaffolds promote the aggregation and osteodifferentiation of human mesenchymal stem cells. Biopolymers 109: e23223. DOI: 10.1002/bip.23223.

Zhang J, Luo X, Barbieri D, Barradas AMC, de Bruijn JD, van Blitterswijk CA, Yuan H (2014) The size of surface microstructures as an osteogenic factor in calcium phosphate ceramics. Acta Biomaterialia 10: 3254-3263. DOI: 10.1016/j.actbio.2014.03.021.

Zhao L, Hantash BM (2011) TGF-β1 regulates differentiation of bone marrow mesenchymal stem cells. Vitamins and Hormones 87: 127-141. DOI: 10.1016/B978-0-12-386015-6.00042-1.

Zhao L, Huang J, Zhang H, Wang Y, Matesic LE, Takahata M, Awad H, Chen D, Xing L (2011) Tumor necrosis factor inhibits mesenchymal stem cell differentiation into osteoblasts via the ubiquitin E3 ligase Wwp1. Stem Cells (Dayton, Ohio) 29: 1601-1610. DOI: 10.1002/stem.703.

Editor's note: The Scientific Editor responsible for this paper was Martin Stoddart.